Progress In Electromagnetics Research B, Vol. 77, 37–55, 2017

Development of an Adaptive Approach for Identification of Targets (Match Box, Pocket Diary and Cigarette Box) under the Cloth with MMW Imaging System

Bambam Kumar, Rohit Upadhyay, and Dharmendra Singh*

Abstract—Non-metallic objects, such as match box and cigarette box, detection and identification are quite an essential task during personal screening from standoff distance to protect the public places like the airport. Although various imaging sensors such as microwave, THz, infrared and MMW with signal processing techniques have been demonstrated by the researchers for concealed weapon detection, it is still a challenging task to detect and identify different types of small size targets such as matchbox, pocket diary and cigarette box simultaneously. Therefore, in this paper, an attempt has been made to develop such an algorithm/methodology by which different types of small targets, such as a matchbox and cigarette box, which is fully or half-filled or empty and pocket diary at different orientations beneath various cloths can be detected and identified with an MMW radar system. For this purpose, an optimal method has been proposed to form an image, and after that, in post processing a novel adaptive approach for detection and identification of considered targets has been proposed. The data were collected by MMW system at V-band (59 GHz–61 GHz). The proposed algorithm/methodology gives a quite satisfactory result.

1. INTRODUCTION

The concealed targets detection and identification beneath different cloths are really desired in view of safety as well as security of the public and their assets, such as airports, shopping malls and playground stadiums. [1]. Gradiometer metal detectors and X-ray scanner have been used for a very long time. The former is most suitable to detect target such as metals and high conductivity materials; however, it is unable to detect target such as match box, and the latter is used to detect concealed targets in luggage box but not in the human body because the ionizing property of x-rays is harmful to human body [2, 3]. Microwave imaging techniques have been used for through-wall imaging (TWI) and ground penetrating radar (GPR) [4, 5]. However, the lower frequency range of microwave imaging technique suffers from very poor resolution [6]. Various researchers have started to work for concealed target detection in the frequency range between microwave and X-ray, which is known as infrared imaging, THz imaging, and millimetre wave imaging (MMW) [7–9]. Nowadays, MMW and THz wave are attracting the attention of researchers because of their high-resolution capability [10]. Resolution is one of the important factors for detection of small targets.

To increase the resolution of MMW image, researchers have demonstrated various signal processing steps for concealed weapon detection, quality monitoring for non-destructive testing (NDT) and medical imaging [9, 11, 12]. However, very limited research work has been reported at 60 GHz centre frequency on the basis of signal processing algorithms for complete concealed target detection and its identification.

Received 8 April 2017, Accepted 28 June 2017, Scheduled 19 July 2017
* Corresponding author: Dharmendra Singh (dharmfec@gmail.com).
The authors are with the Department of Electronics and Communication Engineering, Indian Institute of Technology Roorkee, Roorkee, Uttarakhand, India.

Digital signal processing steps such as clutter and noise removal techniques, segmentation, thresholding and identification for detection and identification are used for camera based images as well as microwave radar imaging, i.e., GPR and TWI [4, 5, 13, 14]. Various signal processing techniques are available, but it is important to critically analyse these techniques for proper use in a particular application. A comparison of different statistics-based clutter reduction techniques is given in [13]. Spatial linear and nonlinear filters, such as Gaussian, mean, mode, median, adaptive median and max filters, have been used to enhance the quality of the image [15]. A variety of segmentation and thresholding techniques have been proposed by researchers for detection of targets, such as histogram based [16], clustering based [17], entropy based thresholding [18], locally adaptive thresholding [19], Hidden Markov model (HMM) [20] and mixture of Gaussian densities with Iso-counters evolution [21]. The performance of any segmentation and thresholding operation largely depends on various factors, such as non-stationary and correlated clutter, ambient illumination and mixing of gray levels within the object and its background [22]. Histogram based technique performs better when the object and background are largely separated and have distinct bimodal valley point. Although Markov model and gaussian model are noise resistant, they are computationally inconsistent. Entropy method performs fairly in uniform images, but it is complex because of logarithmic calculations involved [23].

Further, it is essential to know the specific target material types such as metal, paper, plastic, clothing to identify the targets [24, 25]. A number of different identification techniques have been reported by researchers which are generally used for identification of feature extraction based techniques, artificial neural network (ANN) and material of targets [26, 27]. Shape-based feature extraction is not suitable for identifying targets like match box, cigarette box and pocket diary which have almost similar shape and size.

Statistics based detection and identification has been used for characterization of natural, urban and sea surfaces using synthetic aperture radar and medical field [28–31]. However, very limited research has been reported on statistics based concealed targets identification. Single probability density function classifier has been used to study the changes of gait cadence in amyotrophic lateral sclerosis (ALS) which is a type of neurological disease [32]. Various probability density functions (pdfs) have been used to improve the performance of target detection, despeckling and identification of SAR images [33–35]. The scattering distribution of pdf parameter is highly sensitive to the frequency, range and roughness properties of the targets [36, 37]. A small change in these properties provides a big change in the scattered distribution. Thus, the single probability density based function may fail to capture the true properties of the backscattered signal; hence the false alarms rate may be increased.

Therefore, in this paper, an attempt is made to detect and identify the concealed targets like a match box, pocket diary and cigarette box with MMW wave imaging radar. The paper is organized as follows. Section 2 describes an MMW imaging radar system, data acquisition and pre-processing steps for enhance the quality of the raw image. Section 3 discusses different signal processing techniques used for target detection and identification. Validation of the system is discussed in Section 4, and Section 5 concludes this work.

2. MMW RADAR SYSTEM FOR DATA ACQUISITION AND PRE-PROCESSING

MMW radar has been erected using vector network analyser (make: Agilent N5247A (10 MHz–67 GHz) PNA-X), VNA cable (make: MMW-N4697F (DC to 67 GHz) −1.85 mm) and pyramidal horn antenna (make: MESA MW-HF-907V) in stepped frequency continuous wave (SFCW) mode. In generating the SFCW signal, the frequencies between adjacent sub-signals are increased by an incremental frequency of Δf. For one burst of SFCW signal, a total of 'N' continuous wave signals, each having a discrete frequency of $f_N = f_0 + (N-1) \times \Delta f$, is sent, where f_0 is the frequency of the first signal. The detailed specifications of active millimetre wave imaging radar is given in Table 1.

2.1. Arrangement of Imaging System

Generally, all these selected targets are kept in pocket. The front part of a target is covered with piece of cloth, and the back side of target is human body (Chest). In this case, we replace body part with polystyrene sheet. We consider three different targets which are from three different materials, paper

Table 1. Specifications of active millimeter wave imaging radar for concealed target detection.

MMW Active Radar Parameter	Typical Value
Operating frequency	59 GHz–61 GHz
BW	2 GHz
No. of frequency points (N)	201
Transmitted Power	0 dBm
Range resolution	7.5 cm
Cross range resolution	0.625 cm
Antenna type	Pyramidal Horn
Beam width of antenna (E, H Plane)	9.1 degrees, 10.4 degrees
Gain of antenna	25 dBi
Antenna Swath	0.028 m^2

board for match box, plastic cover for pocket diary, and polythene cover and aluminium foil (outside and inside of cigarette box) whose dielectric value is slightly different from human body. The scattered statistics depends upon dielectric property of targets. The dielectric constant of human skin (palm) is approximately 1.5 at 60 GHz [38]. The dielectric value of normal human breast is approximately 3 at 50 GHz [39, 40]. Therefore, we take polystyrene whose dielectric is in between 2–3 in the considered frequency range [41].

The reflection coefficient (S_{11}) is observed for human body (chest) and polystyrene sheet (thickness 2 cm) which is shown in Figure 1, and it is noticed that the reflection coefficient of polystyrene sheet is nearly the same as human body for frequency range 59 GHz to 61 GHz.

The dielectric constant of the considered polystyrene sheet (thickness 2 cm) is also measured using free space setup [42]. In this method, polystyrene sheet is placed between two antennas, which operates in bistatic mode and measured under a far-field condition. First, the system is calibrated using gated-reflect-line (GRL) calibration method [43]. It is a full two-port calibration method similar to a LRM calibration (Line, Reflect, Match). After calibration, the dielectric constant of polystyrene sheet is calculated using Agilent 85071E Materials Measurement Software that uses Transmission-Reflection-Line (TRL) method [42, 43]. The result is shown in Figure 2. The value of dielectric constant of polystyrene sheet is approximately 2.2 at frequency range (59–61) GHz. Therefore, we take background material as polystyrene in the place of human body.

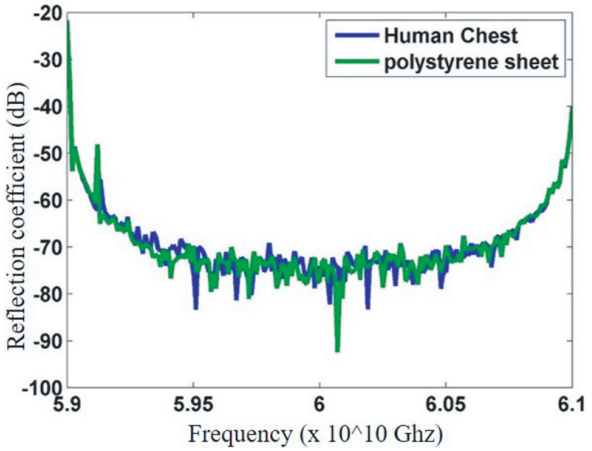

Figure 1. Reflection Coefficient for human body and polystyrene sheet.

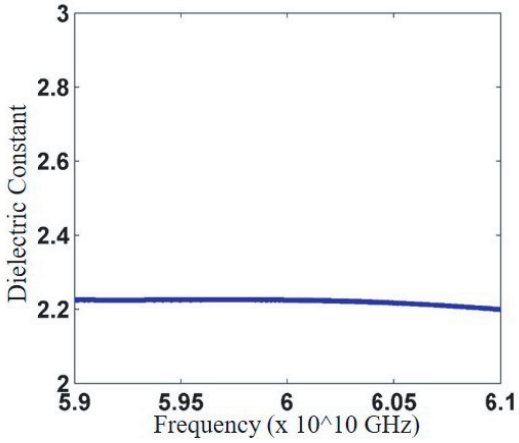

Figure 2. Dielectric constant for considered polystyrene sheet.

The target is placed over a polystyrene sheet of thickness 2 cm because the permittivity of a polystyrene sheet is nearly the same as the permittivity of the human body at 60 GHz. The polystyrene sheet with the target is mounted on a movable 2D wooden scanning frame so that it can be moved by fixed number of steps in horizontal as well as vertical direction as shown in Figure 3. The distance between two consecutive scan positions is kept at 2 cm in both horizontal and vertical directions. The numbers of horizontal and vertical scanning positions are 30 and 16, respectively. The target is placed at a distance of 75 cm from the flare of the antenna. We place the match box at left most position, pocket diary at middle position and cigarette box at right most position, covered by either cotton or woolen cloth for the concealed targets detection as shown in Figure 4. Match box and pocket diary are kept at 6 cm apart, and the separation between a pocket diary and cigarette box is at 4 cm. The orientation of target and quantity of match stick and cigarette inside the box is varied for identification point of view. Details of different targets nomenclature and their corresponding properties, used throughout in this paper, are summarized in Table 2. Full, half and empty denote the level of cigarette and match stick inside cigarette and match box as shown in Table 2 column c. Targets Id T1 to T10 are used for development of concealed target detection and identification, and targets Id V1 to V3 are used for validation purpose of concealed target detection and identification.

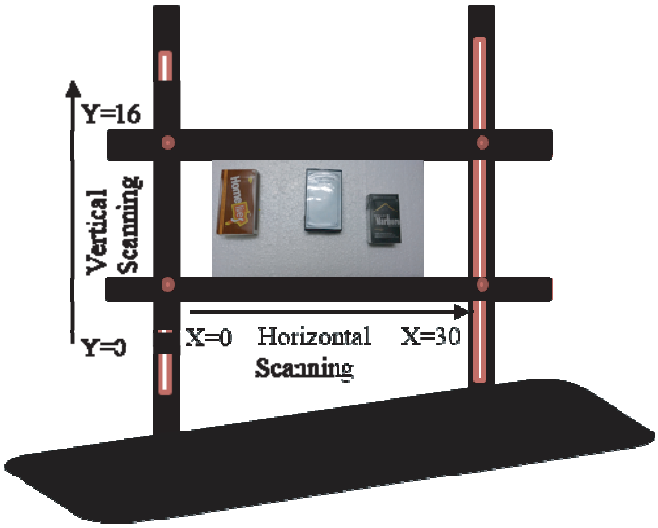

Figure 3. An arrangement of target used for millimetre wave stand-off concealed target detection.

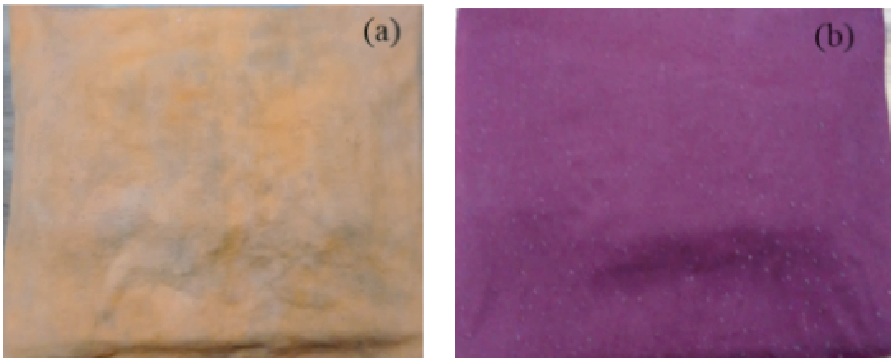

Figure 4. The target used for millimeter wave stand-off concealed target detection and identification. (a) Concealed targets covered with cotton cloth piece. (b) Concealed targets covered with woolen cloth piece.

Table 2. Different targets with target Id and their corresponding properties.

S. No.	Target Id	Quantity Inside MB & CB	Covering material for CB, MB &PD	Orientation
a	**b**	**c**	**d**	**f**
1	**T1**	Full	Cotton	0°
2	**T2**	Full	Woolen	0°
3	**T3**	Half	Cotton	0°
4	**T4**	Half	Woolen	0°
5	**T5**	Empty	Cotton	0°
6	**T6**	Empty	Woolen	0°
7	**T7**	Full	Cotton	60°
8	**T8**	Full	Woolen	60°
9	**T9**	Full	Cotton	45°
10	**T10**	Full	Woolen	45°
11	**V1**	Full	Cotton	0°
12	**V2**	Empty	Woolen	0°
13	**V3**	Full	Cotton	40°
	CB = Cigarette box, PD = Pocket diary and MB = Match box.			

2.2. Data Acquisition and Preprocessing

The complex scattering parameters (S_{11}) are collected at $N = 201$ frequency point in the frequency domain. Several preprocessing steps such as frequency to time domain conversion, time domain to spatial domain conversion and external calibration are applied to obtain range profile of target whose details are given in [27]. It gives range profile information of a target in terms of intensity vs downrange. The cross-range resolution of MMW radar system is 0.625 cm at 60 GHz center frequency [27]. The total 30 horizontal scans are carried out which is also known as B-scan, whose matrix dimension is 201×30. It gives information about down range and width of the target. Stacking of B-scan in the vertical direction at equal step size is called C-scan. The vertical scanning positions are 16, so C-scan data form 3-D matrix whose dimension is $201 \times 30 \times 16$. The total sixty C-scan data are taken, and six sets of reading are taken for each targets Id as shown in Table 2, in which the first fifty sets of data are used for development of the algorithm, and the rest ten are used for validation purpose. The raw C-scan image is shown in Figure 5, where it is very difficult to conclude anything. Therefore, there is a need to develop a methodology by which different targets can be detected and identified. Various techniques of such a type are critically analyzed as given in following steps.

2.2.1. Step 1: Normalization

The raw C-scan image contains a wide variation in reflected intensity values due to different dielectric materials of concealed targets. Therefore, firstly, raw C-scan data are normalized for further processing, such as clutter reduction, segmentation, thresholding and identification. The basis of normalization is to bring image intensity value in one scale; normalization process is applied according to

$$I_{norm} = \frac{I - I_{\min}}{I_{\max} - I_{\min}} \tag{1}$$

where I is the pixel intensity value of the image at any arbitrary location, I_{norm} the normalized pixel intensity, and $I_{\max}$ and $I_{\min}$ are the maximum and minimum intensity values of the raw C-scan image. The normalized images are shown in Figure 6.

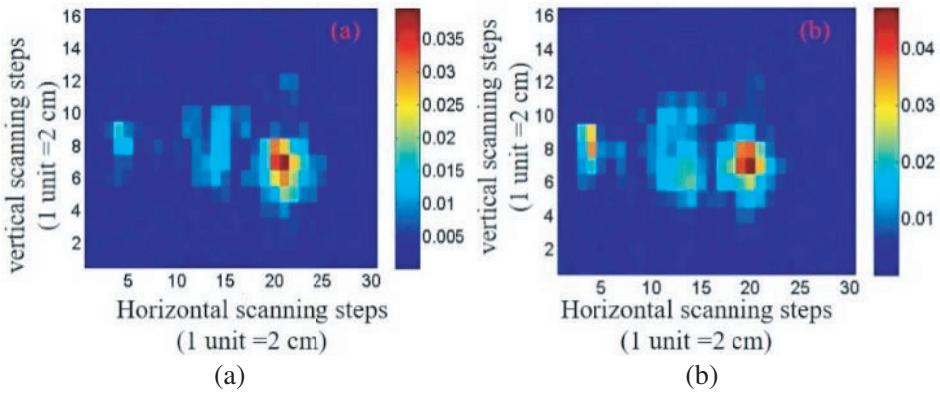

Figure 5. C-scan raw image for concealed targets Id (a) T1 and (b) T2.

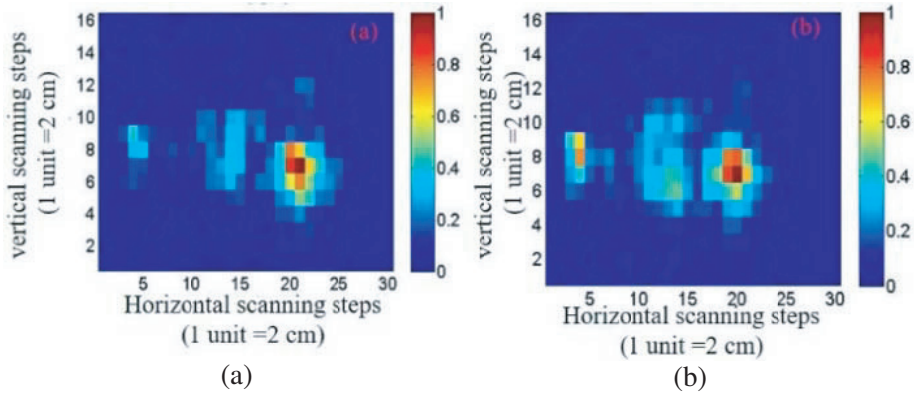

Figure 6. C-scan normalized image for targets Id (a) T1 and (b) T2.

2.2.2. Step 2: Clutter Reduction

The normalized C-scan data have actual information of target as well as clutter signals, such as antenna-air interference signal, reflection and refraction due to multipath propagation, background reflection and covering cloth reflection. Clutter signals are unrelated to target's scattering signal but occur in the same time window. Therefore, several statistics-based clutter removal techniques like, singular value decomposition (SVD), principle component analysis (PCA), factor analysis (FA), independent component analysis (ICA) and average trace subtraction (ATS) have been applied [13]. Out of these many clutter reduction techniques, the best suitable technique is selected on the basis of peak signal to noise ratio (PSNR) as shown in Table 3. PSNR can be calculated using Eqs. (2) and (3) [44].

$$MSE = \frac{1}{MxN}\sum_{i=1}^{N}\sum_{j=1}^{M}\{f(i,j) - p(i,j)\}^2 \tag{2}$$

$$PSNR\,(\text{dB}) = 10\log\left(\frac{1}{MSE}\right) \tag{3}$$

where $f(i,j)$ and $p(i,j)$ are the normalized and clutter removed images, respectively; M and N are dimensions of image; MSE is a mean square error.

SVD decomposes the scattered signal into different unrelated subspaces such as target subspaces and clutter subspaces. SVD is a most reliable and computationally effective matrix decomposition technique which has additional advantages such as better image quality and lower mean square error (MSE) than other statistics-based clutter removal techniques. The normalized image $f(i,j)$, with dimension $M \times N$,

Table 3. Performance of clutter removal techniques on the basis of PSNR for target Id T2.

S. No	Clutter removal techniques	PSNR (dB)
1	SVD	25.95
2	PCA	17.62
3	FA	14.34
4	ICA	16.18
5	ATS	18.41

where $i = 1, 2, 3, \ldots, M$ and $j = 1, 2, 3, \ldots, N$, can be decomposed as [13]

$$f = UDV^T \tag{4}$$

where U and V are unitary matrix such as $UU^T = I$, $V^TV = I$, and D is a diagonal matrix whose elements are $D = \text{diag}(\sigma 1, \sigma 2, \sigma 3, \ldots, \sigma r)$ with $\sigma 1 \geq \sigma 2 \geq \sigma 3 \geq \ldots \geq \sigma r \geq 0$. The diagonal components of D are called singular values, and SVD of function f is

$$f = \sum_{k=1}^{N} \sigma_k u_k v_k^T \tag{5}$$

or

$$f = f_1 + f_2 + f_3 \ldots + f_N \tag{6}$$

where f_i matrix has the same dimensions as f and is called the ith eigen image of f. After analyzing the eigen values, it is found that eigen images $f1$, $f2$ and $f3$ correspond to three different targets, and remaining eigen image represents clutter. Hence target signal can be represented as

$$S = \sum_{k=1}^{3} \sigma_k u_k v_k^T \tag{7}$$

Singular value decomposition method is applied to clutter mitigation according to Equations (4)–(7). It removes clutter by decomposing radar signal into multidimensional subspace due to different dielectric targets, background and surrounding reflections. Results are shown in Table 3, where it is observed that SVD provides the best results. So SVD clutter reduction technique is applied, whose results are shown in Figure 7, which is further processed for enhancement. SVD is very useful for characterizing and analyzing the behavior of scattered signal which is a mixture of target signal and clutter signal

2.2.3. Step 3: Image Enhancement

Spatial convolution filter, adaptive median filter, mean filter and spatial maximum filter are critically analyzed for targets image enhancement [45, 46], and results are compared on the basis of PSNR as shown in Table 4. PSNR is calculated between SVD image and spatial filtered image according to Equations (2)–(3). Out of these several image enhancement techniques, spatial maximum filtering method provides better result to find missing pixel points, and it also enhances the intensity of image pixel. The pixels of an image are modified by moving the filter mask from one pixel point to another pixel point of image in spatial filtering operation. For spatial max filtering operation, 3×3 filter mask is taken, and the middle point of this mask filter is modified by maximum pixel point of filter mask. Therefore, on the basis of PSNR of all filtered images, it is found that spatial max filter provides good results in comparison with the above linear and nonlinear filtering operations, shown in Figure 8. The intensities of pixel points of image are significantly enhanced in target region which is quite helpful to know about the number of targets. The spatial maximum filter also enhances the boundary of targets. These preprocessed image is further used for detection and identification.

Table 4. Performance of spatial filtering techniques on the basis of PSNR for target Id T2.

S. No	Spatial Filter techniques	PSNR (dB)
1	Spatial convolution filter	18.23
2	Adaptive median filter	15.35
3	Mean filter	13.45
4	Spatial maximum filter	20.16

3. POST PROCESSING

3.1. Development of Adaptive Detection and Identification Algorithm for Considered Targets under the Cloths and Its Implementation

3.1.1. Target Detection

To detect the targets, it is important to critically analyze the behavior of individual target and on that basis develop a detection technique. In the considered targets, it is observed that cigarette box, pocket diary and match box have different levels of reflection intensity. For detecting the three types of targets, a proper threshold has to be decided. Detecting and identifying these three targets simultaneously is a very difficult task because of the reflection level. Firstly different commonly used thresholding techniques are critically analyzed

3.1.1.1 Critical Analysis of Commonly Used Thresholding Techniques

The main aim of this task is to demarcate the three different considered targets. For this purpose, statistics based thresholding method, maximum entropy based thresholding method, Otsu's thresholding method and cluster based thresholding are applied [16–19] and analyzed. The performance of these thresholding methods is measured on the basis of true positive (TP) and false positive (FP), which can be defined as [11]

$$TP = \frac{\text{Correctly detected target pixels}}{\text{Total no. of target pixels}} \tag{8}$$

$$FP = \frac{\text{Incorrectly detected target pixels}}{\text{Total no. of pixels-total no. of target pixels that exit}} \tag{9}$$

The total number of each target's pixels can be determined by a priori knowledge about size of target, cross range resolution of MMW imaging system and step size of target movement in horizontal and vertical directions. The sizes of MB and PD are nearly equal to (8×6) cm, and the size of CB is

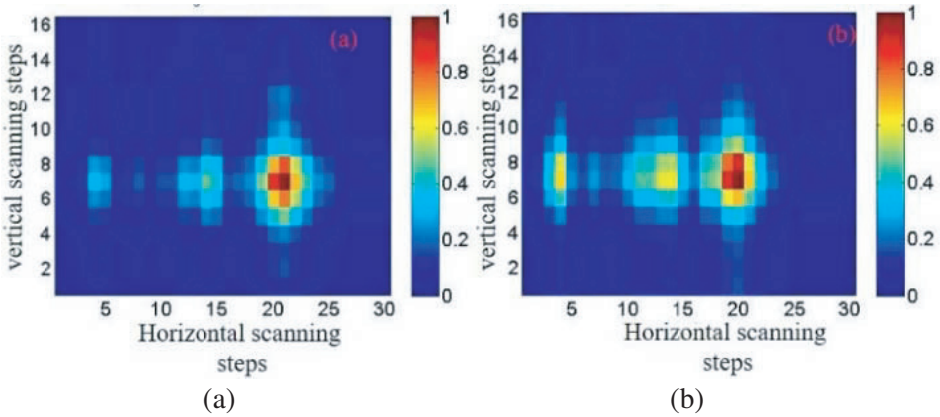

Figure 7. SVD image for concealed targets Id (a) T1 and (b) T2.

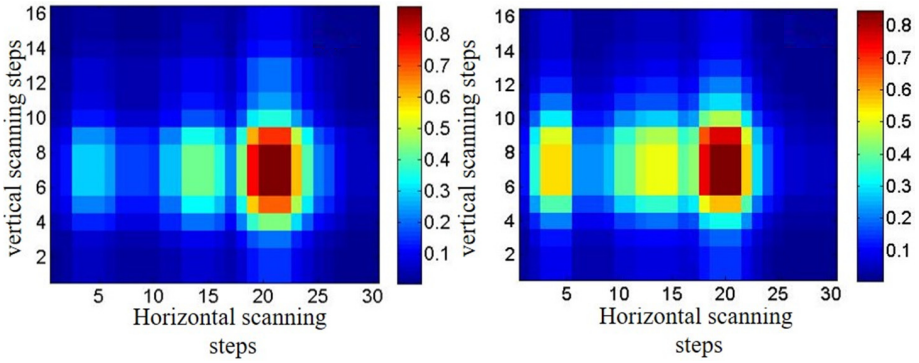

Figure 8. Spatial Max filter image for concealed targets Id (a) T1 and (b) T2.

nearly equal to (10×6) cm which covers approximate $(4 \times 3 = 12)$ and $(5 \times 3 = 15)$ pixels, respectively. The targets region is defined on a priori knowledge of target location and their corresponding size. If the obtained pixel is outside the defined boundary region, then it means false alarm, and no pixel below the boundary region denotes missed pixels point. Table 5 shows the comparison of the performances of all four thresholding techniques in terms of TP and FP for target Id T2. Otsu's method is a very popular global automatic thresholding technique, in which a threshold is determined by maximizing discriminant measure [16]. This method provides missed out pixel points for each class and also false alarm for CB. In cluster-based thresholding methods, an image sample is divided into two parts: one corresponds to background, and the other corresponds to foreground [17]. This method provides missed out pixel points and false alarm for each class. The maximum entropy based thresholding method provides the threshold value by maximizing *a posteriori* entropy that is subject to certain inequality constraints which are derived by means of special measures characterizing uniformity and shape of the regions in the image [18]. This method gives false alarm for all types of considered targets and missed out pixel points for MB and PD. Statistics-based thresholding method provides true target detection for each class but generates false alarm for PD and CB. All these thresholding methods provide either false alarm or missed out pixel point due to wide intensity variation among targets.

Table 5. Performance of thresholding techniques on the basis of TP and FP for target Id T2.

S. No.	Thresholding techniques	True positive (TP)			False positive (FP)		
		MB	PD	CB	MB	PD	CB
1	Statistics-based thresholding	1	1	1	0	0.2	0.4
2	Maximum entropy based thresholding method	0.6	0.7	1	0.3	0.7	0.55
3	Otsu's thresholding	0.4	0.5	0.83	0	0	0.2
4	Cluster based thresholding	0.7	0.91	0.83	0.4	0.33	0.4

From above observation, it is clear that single threshold method is not able to detect complete shape of targets simultaneously because of wide variation in intensity level in images from different types of materials, but statistics-based thresholding methods provide better results than other thresholding methods.

3.1.1.2 Proposed Decision Criterion for Thresholding

Step:1 Critical Analysis of Statistics-Based Thresholding Techniques

The statistics-based threshold method is proposed which can be defined as the function of mean

and standard deviation of the image

$$\text{Th} = f(\text{Mean, Standard deviation}) \tag{10}$$

A wide and extensive investigation has been carried out for choosing the threshold boundary required to detect targets under cloths using image statistics (i.e., mean "μ_A" and standard deviation "σ_D"). It is found that the desired threshold boundary for detection of concealed targets cannot be easily obtained by using separately or mixing the mean and standard deviation of the entire image (i.e., μ_A, σ_D, $\mu_A \pm \sigma_D$). The image statistics may not be exactly the same for two images of a similar situation, Therefore, it is not reasonable to consider expression μ_A, σ_D, $\mu_A \pm \sigma_D$ as the threshold boundary of a selected attribute for the detection of concealed targets. Hence, to make the expression adaptive, an unknown term 'p' is included to form different mathematical expressions (e.g., $\mu_A \pm p * \sigma_D$) for threshold boundary. The statistics-based threshold method can be defined as

$$\text{Th} = \mu_A - p * \sigma_D \tag{11}$$

The statistics-based thresholding technique should work in such a manner that it maximizes the accuracy of detection and concurrently minimizes the false alarm. For this, optimizing the value of 'p' is needed so that the goal may be achieved. In order to achieve the goal, firstly, compute the true positive (TP) and false positive (FP) values of the obtained image. They are defined in Equations (8) and (9), respectively.

The true positive value provides the overall accuracy, and false positive value gives the false alarm. These two parameters are related to the scaling parameter 'p'. Here, for four randomly selected different targets Id, TP and FP are plotted for different values of p as shown in Figures 9 and 10. It is observed that the values of TP and FP increase with increasing 'p', and after a definite critical value of 'p', TP approaches the desired true positive value, i.e., 1. On the other hand, the false alarm also increases after increasing the value of 'p' as shown in Figure 10. This compromising behavior of TP and FP is required to be stable. Therefore, we need to select optimum value of 'p' that offers maximum overall accuracy and at the same time minimal false alarm.

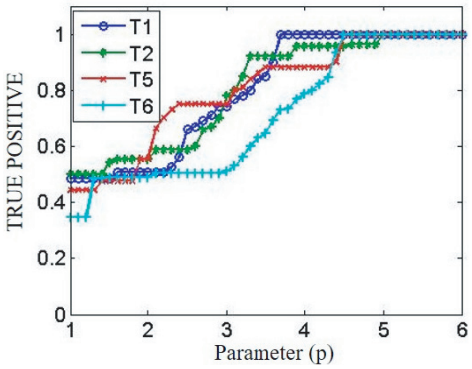

Figure 9. Plot of True positive vs p of concealed targets for target Id T1, T2, T5and T6.

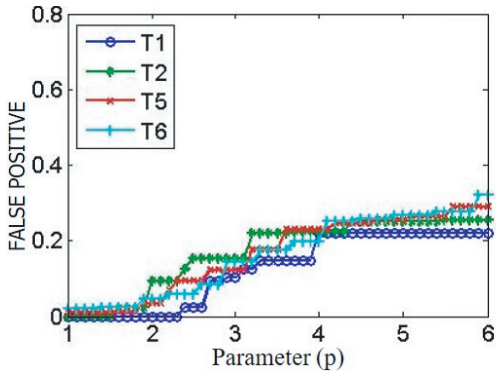

Figure 10. Plot of False positive vs p of concealed for target Id T1, T2, T5 and T6.

Step 2. Formulation for Optimization the Scaling Parameter (p)

The curve-fitting approach is used for developing an empirical relation between TP and FP with 'p', shown in Figures 9 and 10. Several relations are analyzed, and the following empirical relations are selected on the basis of coefficient of determination (R^2) values which are 0.9 for both the relations:

$$\text{TP}\,(p) \;=\; a1 \exp - \left(\frac{\mu_A - p * \sigma_D - b1}{c1} \right)^2 \tag{12}$$

$$\text{FP}\,(p) \;=\; a2 \exp - \left(\frac{\mu_A - p * \sigma_D - b2}{c2} \right)^2 \tag{13}$$

where, $a1$, $a2$, $b1$, $b2$, $c1$ and $c2$ are constants. The values of the constants are given in Table 6 for both TP(p) and FP(p). Multiple sets of observations are taken for single set of target Id as shown in Table 2, in which one set of observations is shown in Table 6.

Table 6. Constant value of TP and FP with corresponding R^2 values for different targets Id.

Target Id	a1	b1	c1	$\mathbf{R^2}$	a2	b2	c2	$\mathbf{R^2}$
T1	.9968	.4727	2.53	0.9234	10.6	−2.301	2.824	0.9597
T2	1.644	−1.126	3.26	0.9243	5.757	−2.389	2.727	0.9777
T3	1.067	1.789	1.781	0.9369	8.692	−0.680	1.828	0.9683
T4	1.042	1.58	1.705	0.9651	10.99	−1.021	1.941	0.9711
T5	1.134	2.311	2.072	0.8854	0.0532	0.103	2.097	0.9641
T6	1.134	2.28	2.021	0.8624	0.3939	−3.86	3.707	0.9391
T7	1.003	0.4849	2.409	0.9398	0.08093	−0.73	2.4	0.956
T8	1.093	1.82	1.568	0.9581	3.169	0.583	1.372	0.9747
T9	14.31	−6.52	4.714	0.9414	0.0149	0.738	13.48	0.9657
T10	0.968	1.753	2.063	0.8858	10.99	−1.021	1.654	0.9711
Average value	2.439	0.4844	2.412	0.9222	5.07	−1.057	3.403	0.9647

After deriving the empirical relation of TP(p) and FP(p) with 'p', next step is to find the best value of 'p' so that true positive value and false positive value are maximized and minimized, respectively. For this purpose, genetic algorithm (GA) is used.

The values of $a1$, $b1$, $c1$, $a2$, $b2$ and $c2$ of Equations (12) and (13) are replaced by the average values as shown in Table 6. As shown in Figures 9 and 10, by maximizing TP(p), FP(p) is also maximized and vice versa. This type of problem can be solved as a multi-objective optimization problem for value of 'p' in the range between 1 and 6. In genetic optimization algorithm problem, function $Y(p)$ is divided into two vector functions, i.e., $Y_1(p)$ and $Y_2(p)$, which corresponds to true positive function whose value should be near one and false positive function whose value should be close to zero, respectively. $Y_1(p)$ and $Y_2(p)$ are defined as

$$\text{Minimizing } Y(p) = [Y_1(p), Y_2(p)]; \quad 1 < p < 6 \quad \text{Such that} \quad Y_1(p) = -\text{TP}(p) \text{ and } Y_2(p) = \text{FP}(p)$$

Our main focus is to maximize TP(p) and minimize FP(p) for optimum value of p. For that, the goal is set such that FP should be lower than the upper boundary (ub_{TN}) and TP greater than the lower boundary (lb_{TP}). The goal vector can be defined as

$$\text{Goal} = [-ub_{\text{TN}} ub_{\text{TN}}] \text{ for fitness function } Y(p) = [Y_1(p), Y_2(p)];$$

This gives the critical value of p so that TP $> lb_{\text{TP}}$ and FP $< ub_{\text{TN}}$. The developed algorithms are tested for unknown targets as shown in Table 7. Figure 11 shows the statically based thresholded image for targets Id V1 and V2, which are independent data sets and never used for training the algorithm.

Table 7. Values of scaling parameter "p" for unknown targets Id with TP and FP.

Targets Id	Mean ($\mu_{\mathbf{A}}$)	Std. Dev. ($\sigma_{\mathbf{D}}$)	p	TP	FP
V1	0.3634	0.0217	4.1	1	0.13
V2	0.5766	0.0342	4.3	1	0.05

After target detection, the next step is target identification. For target identification, the first image segmentation technique is applied so that individual target pixels can be analyzed properly.

Step 3. Segmentation of Image

Segmentation is done on the basis of the fusion of normalized image (Figure 6) and thresholded image (Figure 11). The thresholded image gives approximately correct boundary of the considered targets. Now the image is segmented in three parts, and the number of corresponding target pixels are extracted. Now the second objective is identification of targets, and these segmented pixels may be quite helpful for identification of targets.

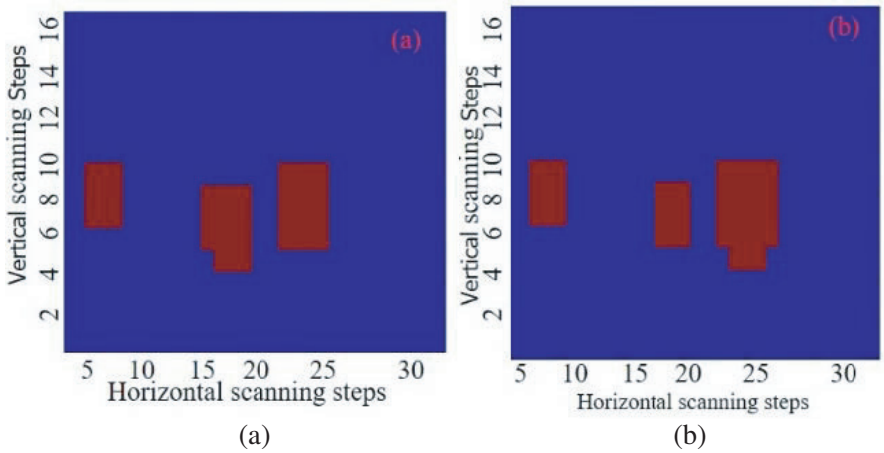

Figure 11. Image for target Id (a) V1 and (b) V2 with proposed threshold technique.

3.1.2. Proposed Technique for Target Identification

After targets detection, the next objective is target's identification. Three separate regions of normalized image, as shown in Figure 6, obtained corresponding to three different targets, are used for targets identification on the basis of statistics. The identification is performed on the basis of statistical distribution of reflected data. As discussed above, scattered statistics depend upon several parameters, such as dielectric property and roughness of targets. Therefore, multivariate classes are observed of normalized image due to different types of materials and roughness of the targets. Probability density function is a very useful tool to identify targets around large intensity difference between targets and background. Probability density function has unique features to provide different parameter values for multivariate class, and these parameter values are taken into account for identification purposes. Therefore, for target's identification, various probability density functions were applied on segmented normalized data for finding of different materials, such as paper board for match box, plastic cover for pocket diary, and polythene cover and aluminum foil, outside and inside of cigarette box. Firstly, chi-squared goodness of fit test is performed for all data on more than 50 probability density functions, which were available in easy fit software, and only these pdf functions, namely, normal, Weibull, gamma, Cauchy, Laplace and Rayleigh, pass the chi-square test for all targets on the basis that statistic value should be less than critical value and that p-value is greater than the level of significance (5%) as shown in Table 8 [27]. Out of these pdf functions, the best fit pdfs on the basis of minimum statistic value are selected, which are Laplace, normal and gamma pdf as shown in Table 8.

The best-fit pdfs' distributions (Laplace, normal and gamma pdf) using x as pixel intensity are given below [47].

- Laplace pdf distribution

$$f(x) = \frac{\lambda}{2}\exp(-\lambda|x-\mu|) \tag{14}$$

where μ is the continuous location parameter and λ the continuous scale parameter. The expected (mean) value of a Laplace distribution is

$$E(x) = \mu \tag{15}$$

and the variance is

$$Var(x) = 2/\lambda^2 \tag{16}$$

- Normal pdf distribution

$$f(x) = \frac{1}{\sqrt{2\pi\sigma^2}}\exp\left(\frac{-(x-\mu)^2}{2\sigma^2}\right) \tag{17}$$

$$Var(x) = \sigma^2 \tag{18}$$

Table 8. Chi-squared statistics for various distributions for single target Id T1.

Pdf	Parameters	CB	PD	MB
Normal	Statistics	1.112	0.148	1.811
	P-value	0.726	0.928	0.404
	Critical value	7.814	5.991	5.991
Weibull	Statistics	1.133	1.016	2.569
	P-value	0.889	0.797	0.276
	Critical value	9.487	7.814	5.991
Cauchy	Statistics	2.033	1.798	1.463
	P-value	0.565	0.615	0.690
	Critical value	7.814	7.814	7.814
Laplace	Statistics	0.220	0.180	0.003
	P-value	0.638	0.913	0.984
	Critical value	3.841	5.991	3.841
Rayleigh	Statistics	3.112	1.525	1.525
	P-value	0.210	0.466	0.466
	Critical value	5.991	5.991	5.991
Gamma	Statistics	0.408	0.647	0.001
	P-value	0.981	0.885	0.967
	Critical value	9.487	7.814	3.841

where μ is the continuous location parameter and σ the continuous scale parameter.

- Gamma pdf distribution

$$f(x) = \frac{1}{\beta^{\alpha}\Gamma(\alpha)} x^{\alpha-1} e^{\frac{-x}{\beta}} \tag{19}$$

where α is the shape parameter and β the scale parameter. Both α and β must be greater than zero, and $\Gamma(\alpha)$ is the gamma function and evaluated as

$$\Gamma(\alpha) = \int_0^{\infty} x^{\alpha-1} e^{-x} dx \tag{20}$$

The shape parameter (α) and scale parameter (β) are denoted as

$$\alpha = \frac{(E[x])^2}{Var[x]} \tag{21}$$

$$\beta = \frac{Var[x]}{E[x]} \tag{22}$$

Figure 12 shows comparative plots of the three target material classes for three best-fit pdfs, i.e., Laplace, normal and gamma for target Id T1. Similar plots are also achieved by other target Id. These pdfs are characterized on the basis of location, shape and scale parameter. Location parameter gives the information about location or shift of the distribution. The shape parameter is also called

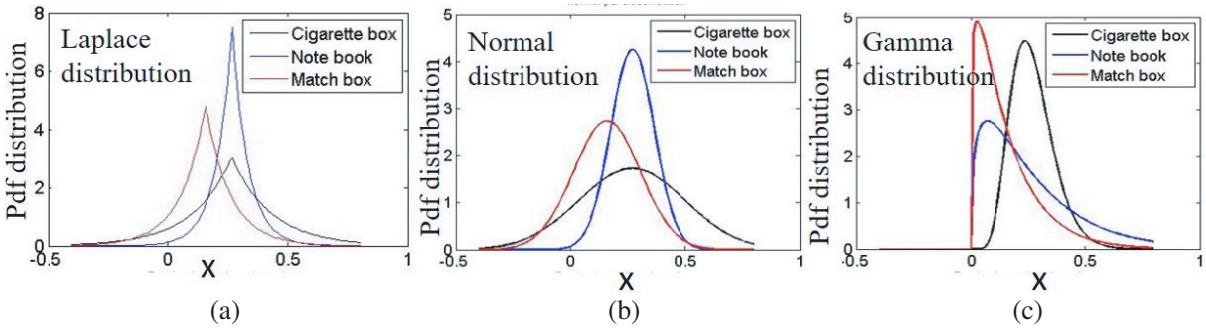

Figure 12. Comparative pdf for three target's class CB, PD and MB. (a) Laplace pdf. (b) Normal pdf. (c) Gamma pdf, for target Id T1.

Table 9. Scale parameters as well as its mean and standard deviation values of Laplace, Normal and Gamma PDF for different targets Id.

Target Id	Laplace scale parameter			Normal scale parameter			Gamma scale parameter		
	CB	PD	MB	CB	PD	MB	CB	PD	MB
	$\lambda 1$	$\lambda 2$	$\lambda 3$	$\sigma 1$	$\sigma 2$	$\sigma 3$	$\beta 1$	$\beta 2$	$\beta 3$
T1	6.550	14.29	10.09	0.215	0.098	0.140	0.200	0.069	0.138
T2	6.548	13.40	11.85	0.215	0.105	0.120	0.205	0.080	0.102
T3	6.001	14.24	11.39	0.235	0.099	0.124	0.229	0.076	0.106
T4	6.151	15.36	11.96	0.229	0.092	0.118	0.230	0.068	0.107
T5	5.670	13.90	10.26	0.249	0.101	0.137	0.193	0.040	0.1326
T6	6.390	15.16	10.96	0.222	0.093	0.130	0.186	0.054	0.1506
T7	5.961	13.85	10.93	0.236	0.102	0.130	0.182	0.050	0.1542
T8	6.470	12.70	9.77	0.218	0.111	0.144	0.199	0.068	0.1322
T9	6.480	14.55	10.37	0.218	0.097	0.136	0.210	0.058	0.1218
T10	6.122	13.09	10.79	0.230	0.108	0.131	0.189	0.053	0.1450
Mean (M)	6.234	14.05	10.83	0.227	0.101	0.131	0.202	0.616	0.1289
Std. Dev. (D)	0.299	0.851	0.735	0.011	0.006	0.008	0.016	0.012	0.0190

slope parameter which gives information about the changes in pdf distribution, whether the function will increase, remain constant or decrease with x. The scale parameter is a measure of spread in distribution in data, i.e., where the bulk of distribution lies. From Figure 12, it is observed that cigarette box and pocket dairy data have wider and narrower pdf plots than match box, and it is common in all three best-fit probability density functions. Therefore, scale parameters (λ, σ and β) are selected for material identification. The scale parameter values of each pdf are calculated according to Equations (16), (18) and (22) for considered targets (Table 2) whose values are shown in Table 9.

Mean and standard deviation of scale parameter for each considered target are computed for defining the range of scale parameter by which the considered targets can be identified. For this purpose, Mean $\pm$ n $*$ Std.Dev is considered while changing the value of n from 0 to 4 at the interval of 0.5. It is observed that at $n = 2$, the scale parameter provides clear demarcation among targets (i.e., no

overlapping of values) which is shown in Table 10.

The identification of target's material is based on any two or more than two combinations of best-fit pdfs. Figure 13 shows a complete flow chart of targets identification.

Table 10. Range of scale parameter of Laplace, Normal and Gamma PDF for target identification.

Target	Laplace Scale Parameter(λ)		Normal Scale Parameter(σ)		Gamma Scale Parameter(β)	
	Min.	Max.	Min.	Max.	Min.	Max.
CB	5.63	6.84	0.205	0.249	0.170	0.234
PD	12.35	15.75	0.089	0.113	0.037	0.085
MB	9.36	12.30	0.115	0.147	0.090	0.167

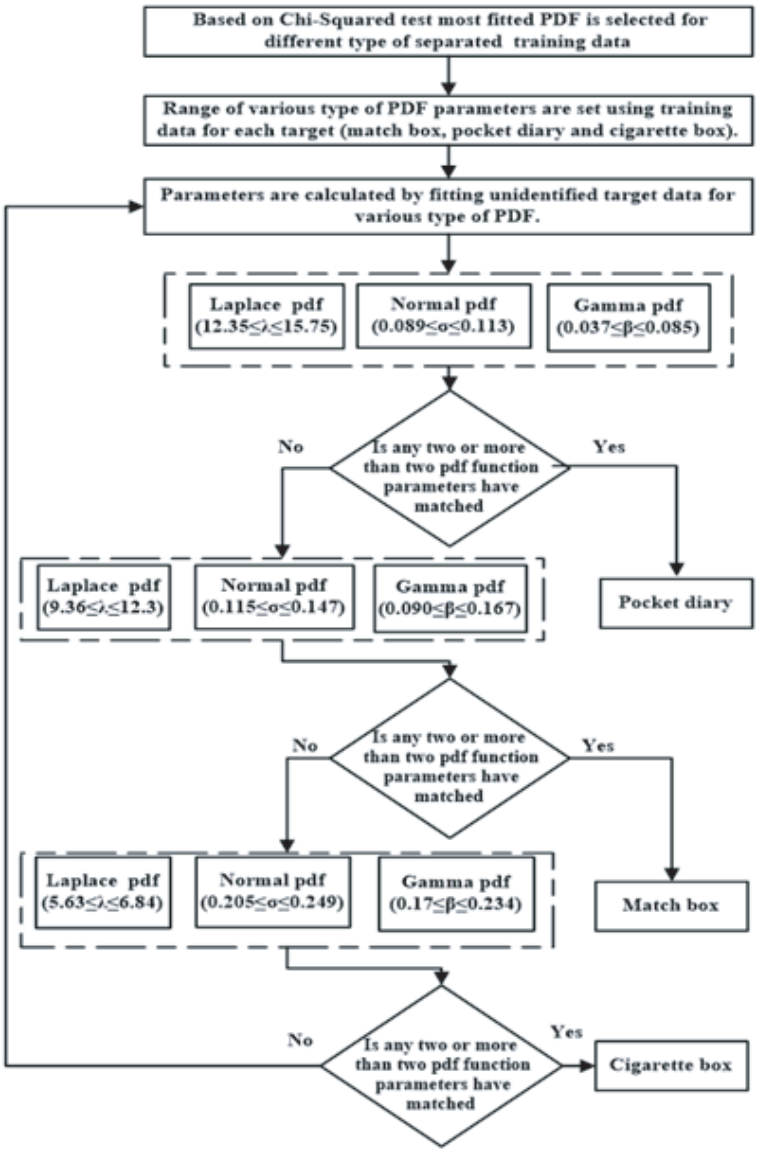

Figure 13. Flow chart of targets identification using probability density function (pdf) based decision tree.

4. VALIDATION FOR DETECTION AND IDENTIFICATION

Final flow chart is shown in Figure 14, and it is validated for 10 different data sets in which 3 data set results are shown in Table 11, and it is observed that the obtained values of ($\lambda 1$, $\sigma 1$, $\beta 1$), ($\lambda 2$, $\sigma 2$, $\beta 2$) and ($\lambda 3$, $\sigma 3$, $\beta 3$) satisfy the respective criteria by which target can be identified as CB, PD and MB successfully.

Table 11. Value of scale parameter for validation of data for target identification.

Target Id	Laplace scale parameter			Normal scale parameter			Gamma scale parameter		
	CB	PD	MB	CB	PD	MB	CB	PD	MB
	$\lambda 1$	$\lambda 2$	$\lambda 3$	$\sigma 1$	$\sigma 2$	$\sigma 3$	$\beta 1$	$\beta 2$	$\beta 3$
V1	6.80	12.55	10.67	0.205	0.112	0.132	0.209	0.084	0.143
V2	6.67	12.81	10.26	0.212	0.110	0.137	0.193	0.055	0.145
V3	6.01	13.42	9.51	0.235	0.105	0.146	0.172	0.077	0.154

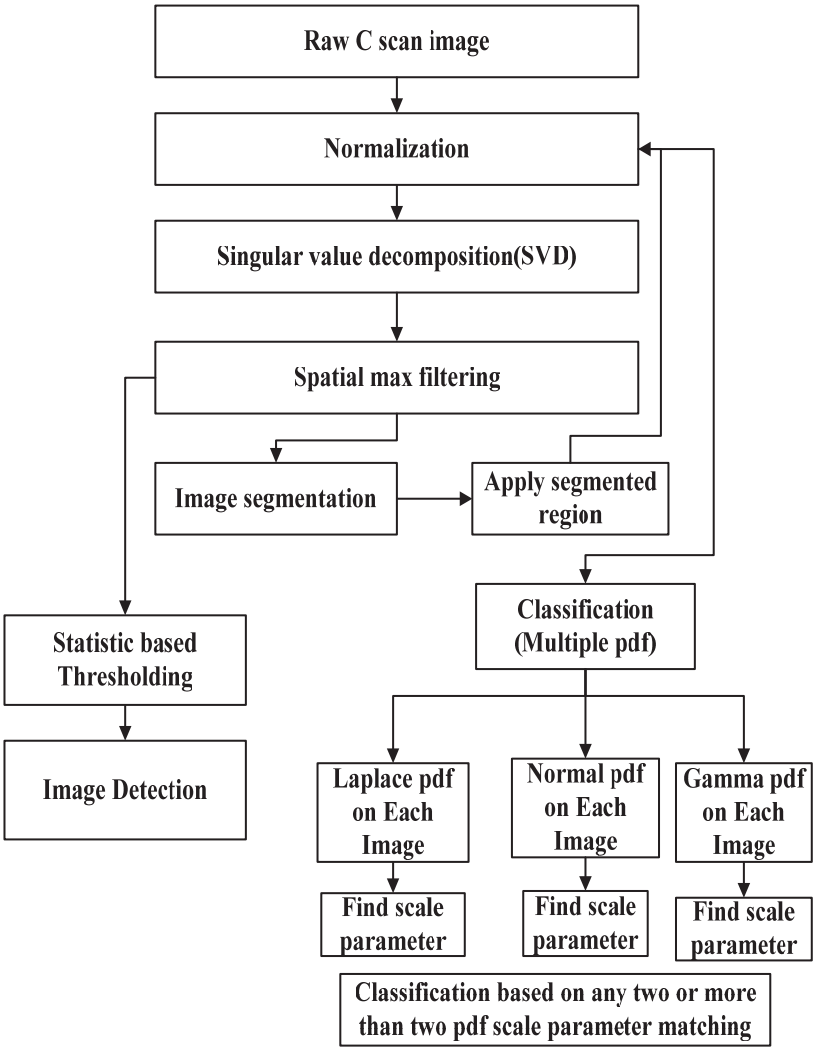

Figure 14. Flow chart of complete signal processing steps for concealed target detection.

5. CONCLUSION

An active MMW SFCW imaging radar system is ingeniously assembled to detect and identify small targets such as match box, pocket diary and cigarette box under different cloths, which operates at center frequency 60 GHz. An optimal preprocessing method is proposed to obtain the image after an adaptive detection and identification algorithm is proposed which gives quite satisfactory results for detecting and identifying the considered targets. The novelty of this paper is to identify the targets which haves different types of materials.

REFERENCES

1. Boris, K. and E. Moshe, "Detecting concealed objects on human body using active millimeter wave sensor," *IEEE Journal on Sensors*, Vol. 10, 1746–1752, 2010.
2. Allen, G. I., P. Czipott, R. Matthews, and R. H. Koch, "Initial evaluation and follow on investigation of the quantum magnetics laboratory prototype, room temperature gradiometer for ordnance location," *Proceedings of the SPIE*, Vol. 3711, 103–112, April 1999.
3. Berrah, N., L. Fang, T. Osipov, B. Murphy, P. Juranic, E. Kukk, K. Ueda, R. Feifel, P. van der Meulen, P. Salen, H. Schmidt, R. Thomas, M. Larsson, R. Richter, K. C. Prince, J. D. Bozek, C. Bostedt, S. Wada, M. Piancastelli, M. Tashiro, M. Ehara, and F. Tarantelli, "Ultraintense x-ray induced multiple ionization and double core-hole production in molecules," *Proc. Conf. Lasers Electro-Opt.*, 1–2, 2011.
4. Hichem, F. and G. Paul, "Detection and discrimination of land mines in ground penetrating radar based on edge histogram descriptors and a possibilistic K-nearest neighbour classifier," *IEEE Transactions Fuzzy System*, Vol. 17, 185–199, 2009.
5. Dionisio, C. R. P., S. Tavares, M. Perotoni, and S. Kofuji, "Experiments on through-wall imaging using ultra-wideband radar," *Microwave and Optical Technology Letters*, Vol. 54, 339–344, 2012.
6. Harmer, S. W., N. Bowring, D. Andrews, et al., "A review of nonimaging stand-off concealed threat detection with millimeter-wave radar [application notes]," *IEEE Microw. Mag.*, Vol. 13, No. 1, 160–167, 2012.
7. Chen, H.-M., S. Lee, R. M. Rao, M.-A. Slamani, and P. K. Varshney, "Imaging for concealed weapon detection: A tutorial overview of development in imaging sensors and processing," *IEEE Signal Processing Magazine*, Vol. 22, 52–61, 2005.
8. Shen, X., C. R. Dietlein, E. Grossman, Z. Popovic, and F. G. Meyer, "Detection and segmentation of concealed objects in Terahertz images," *IEEE Transactions on Image Processing*, Vol. 17, 2465–2475, 2008.
9. Boris, K. and E. Moshe, "Detecting concealed objects on human body using active millimeter wave sensor," *IEEE Journal on Sensors*, Vol. 10, 1746–1752, 2010.
10. Appleby, R. and H. B. Wallace, "Standoff detection of weapons and contraband in the 100 GHz to 1 THz region," *IEEE Transactions on Antennas and Propagation*, Vol. 55, 2944–2956, 2007.
11. Agarwal, S. and D. Singh, "An adaptive statistical approach for nondestructive underline crack detection of ceramic tiles using millimeter wave imaging radar for industrial application," *IEEE Journal on Sensors*, Vol. 99, 1–8, 2015.
12. Chahat, N., M. Zhadobov, R. Sauleau, and S. I. Alekseev, "New method for determining dielectric properties of skin and phantoms at millimeter waves based on heating kinetics," *IEEE Transactions on Microwave Theory and Techniques*, Vol. 60, 827–832, 2012.
13. Gaikwad, A. N., R. Chandra, D. Singh, and M. J. Nigam, "An approach to remove the clutter and detect the target for ultra-wideband through-wall imaging," *Journal of Geophysics and Engineering*, No. 5, 412–419, 2008.
14. Raffaele, S. and C. Antonio, "Front wall clutter rejection methods in TWI," *IEEE Transactions on Geoscience and Remote Sensing Letters*, Vol. 11, 1158–1162, June 2014.
15. Gonzalez, R. C. and R. E. Woods, *Digital Image Processing*, 3rd Edition, Prentice-Hall, Inc., 2006.

16. Otsu, N., "A threshold selection method from gray level histograms," *IEEE Transactions on Systems, Man and Cybernetics*, Vol. 9, 62–66, 1979.
17. Celenk, M., "Colour image segmentation by clustering," *IET Journals & Magazines on Computers and Digital Techniques*, Vol. 138, 368–376, 1991.
18. Wong, A. K. C. and P. K. Sahoo, "A gray level threshold selection method based on maximum entropy principle," *IEEE Transactions on Systems, Man, and Cybernetics*, Vol. 19, 866–871, 1989.
19. Lie, W. N., "Automatic target segmentation by locally adaptive image thresholding," *IEEE Transactions on Image Processing*, Vol. 4, 1036–1041, 1995.
20. Haworth, C. D., B. G. González, M. Tomsin, R. Appleby, P. R. Coward, A. R. Harvey, et al., "Image analysis for object detection in millimetre-wave images," *European Symposium on Optics and Photonics for Defence and Security*, 117–128, 2004.
21. Shen, X., C. R. Dietlein, E. Grossman, Z. Popovic, and F. G. Meyer, "Detection and segmentation of concealed objects in Terahertz images," *IEEE Transactions on Image Processing*, Vol. 17, 2465–2475, 2008.
22. Lee, S. U., S. Y. Chung, and R. H. Park, "A comparative performance study of several global thresholding techniques for segmentation," *Computer Vision, Graphics, and Image Processing*, Vol. 52, 171–190, 1990.
23. Pal, N. R. and S. K. Pal, "A review on image segmentation techniques," *Pattern Recognition*, Vol. 26, 1277–1294, 1993.
24. Krebs, C., P. Warok, S. Heinen, R. Brauns, A. Hommes, S. Kose, et al., "The development of a compact millimeter wave scanning system," *36th International Conference on Infrared, Millimeter and Terahertz Waves (IRMMW-THz)*, 1–2, 2011.
25. Martinez, O., L. Ferraz, X. Binefa, I. Gómez, and C. Dorronsoro, "Concealed object detection and segmentation over millimetric waves images," *IEEE Computer Society Conference on Computer Vision and Pattern Recognition Workshops (CVPRW)*, 31–37, 2010.
26. Deselaers, T., D. Keysers, and H. Ney, "Features for image retrieval: An experimental comparison," *Information Retrieval*, Vol. 11, 77–107, 2008.
27. Agarwal, S., A. Bisht, D. Singh, and N. P. Pathak, "A novel neural network based image reconstruction model with scale and rotation invariance for target identification and identification for active millimetre wave imaging," *Journal of Infrared, Millimetre, and Terahertz Waves*, Vol. 35,1045–1067, Springer, 2014.
28. Li, H.-C., W. Hong, Y.-R. Wu, and P.-Z. Fan, "An efficient and flexible statistical model based on generalized Gamma distribution for amplitude SAR images," *IEEE Transactions on Geoscience and Remote Sensing*, Vol. 48, 2711–2722, 2010.
29. Nick, K. and R. A.-S. Mahmood, "Non-Gaussian target detection in sonar imagery using the multivariate laplace distribution," *IEEE Journal of Oceanic Engineering*, Vol. 40, 452–464, 2015.
30. Abhirup, B. and M. Pradipta, "Rough sets and stomped normal distribution for simultaneous segmentation and bias field correction in brain MR images," *IEEE Transactions on Image Processing*, Vol. 24, 5764–5776, 2015.
31. Cobb, J., K. Slatton, and G. Dobeck, "A parametric model for characterizing seabed textures in synthetic aperture sonar images," *IEEE J. Ocean. Eng.*, Vol. 35, No. 2, 250–266, April 2010.
32. Wu, Y. and S. C. Ng, "A PDF-based identification of gait cadence patterns in patients with amyotrophic lateral sclerosis," *32nd Annual International Conference of the IEEE EMBS Argentina*, 1304–1307, 2010.
33. Banerjee, A., P. Burlina, and R. Chellappa, "Adaptive target detection in foliage-penetrating SAR images using alpha-stable models," *IEEE Transactions on Image Processing*, Vol. 8, No. 12, 1823–1831, December 1999.
34. Achim, A., E. E. Kuruoglu, and J. Zerubia, "SAR image filtering based on the heavy-tailed Rayleigh model," *IEEE Transactions on Image Processing*, Vol. 15, 2686–2693, 2006.
35. Tison, C., J. M. Nicolas, F. Tupin, and H. Maitre, "New statistical model for Markovian identification of urban areas in high-resolution SAR images," *IEEE Trans. Geosci. Remote Sens.*,

Vol. 42, No. 10, 2046–2057, 2004.

36. Stanic, S. and E. Kennedy, "Reverberation fluctuation from a smooth seafloor," *IEEE J. Ocean. Eng.*, Vol. 18, 95–99, 1993.
37. Stanic, S., R. Goodman, K. Briggs, N. Choliros, and E. Kennedy, "Shallow-water bottom reverberation measurements," *IEEE J. Ocean. Eng.*, Vol. 23, 203–210, 1998.
38. Ghodgaonkar, D. K., O. P. Gandhi, and M. F. Iskander, "Complex permittivities of human skin in vivo in the frequency band 26.5–60 GHz," *Proceedings of IEEE Antennas and Propagation Symposium*, Vol. 2, 1100–1103, USA, 2000.
39. Martellosio, A., et al., "0.5–50 GHz dielectric characterization of breast cancer tissues," *Electron. Lett.*, Vol. 51, No. 13, 974–975, June 2015.
40. Martellosio, A., et al., "Dielectric properties characterization from 0.5 to 50 GHz of breast cancer tissues," *IEEE Trans. Microw. Theory Techn.*, Vol. 65, 998–1011, March 2017.
41. Balanis, A., "Measurements of dielectric constants and loss tangents at E-band using a Fabry-Perot interferometer," *NASA Technical Notes NASA TN D-5583*, December 1969.
42. Ghodgaonkar, D. K., V. V. Varadan, and V. K. Varadan, "A free-space method for measurement of dielectric constants and loss tangents at microwave frequencies," *IEEE Trans. Instrum. Meas.*, Vol. 38, No. 3, 789–793, June 1989.
43. Agilent 85071E Materials Measurement Software, Agilent Technologies, Inc., Clara, CA, USA, 2012.
44. Yoo, J. C. and C. W. Ahn, "Image matching using peak signal-to-noise ratio-based occlusion detection," *IET Image Process.*, Vol. 6, 483–495, 2012.
45. Stefan, S., J. E. Wildberger, R. Rainer, N. Matthias, K. R. Klaus, and F. Thomas, "Spatial domain filtering for fast modification of the tradeoff between image sharpness and pixel noise in computed tomography," *IEEE Transactions on Medical Imaging*, 846–853, Vol. 22, 2003.
46. Luis, M. S. B. and B. Eusebio, "Uncertainty estimation by convolution using spatial statistics," *IEEE Transactions on Image Processing*, Vol. 15, 3131–3137, 2006.
47. Walck, C., "Hand-book on STATISTICAL DISTRIBUTIONS for experimentalists," *Internal Report SUF-PFY/96-01*, Particle Physics Group Fysikum, University of Stockholm, 2007.